Published in final edited form as:
Cancer Cell. 2012 August 14; 22(2): . doi:10.1016/j.ccr.2012.06.014.

Therapeutic effect of γ-secretase inhibition in *Kras*^{G12V}-driven non-small cell lung carcinoma through derepression of DUSP1 phosphatase and inhibition of ERK

Antonio Maraver[1,*], **Pablo J. Fernández-Marcos**[#1], **Daniel Herranz**[#1,9], **Maribel Muñoz-Martin**[1], **Gonzalo Gomez-Lopez**[2], **Marta Cañamero**[3], **Francisca Mulero**[4], **Diego Megías**[5], **Marta Sanchez-Carbayo**[6], **Jie Shen**[7], **Montserrat Sanchez-Cespedes**[8], **Teresa Palomero**[9], **Adolfo Ferrando**[9], and **Manuel Serrano**[1,*]

[1]Tumor Suppression Group, Spanish National Cancer Research Center (CNIO), Madrid, Spain

[2]Bioinformatics Unit, Spanish National Cancer Research Center (CNIO), Madrid, Spain

[3]Comparative Pathology Unit, Spanish National Cancer Research Center (CNIO), Madrid, Spain

[4]Molecular Imaging Unit, Spanish National Cancer Research Center (CNIO), Madrid, Spain

[5]Confocal Microscopy Unit, Spanish National Cancer Research Center (CNIO), Madrid, Spain

[6]Tumor Markers Group, Spanish National Cancer Research Center (CNIO), Madrid, Spain

[7]Center for Neurologic Diseases, Brigham and Women's Hospital and Harvard Medical School, Boston, MA, USA

[8]Cancer Epigenetics and Biology Program – IDIBELL, Barcelona, Spain

[9]Institute of Cancer Genetics, Columbia University Medical Center, New York, NY, USA

[#] These authors contributed equally to this work.

SUMMARY

Here, we have investigated the role of the Notch pathway in the generation and maintenance of *Kras*^{G12V}-driven non-small cell lung carcinomas (NSCLCs). We demonstrate by genetic means that γ-secretase and RBPJ are essential in the formation of NSCLCs. Importantly, pharmacologic treatment of mice carrying autochthonous NSCLCs with a γ-secretase inhibitor (GSI) blocks cancer growth. Treated carcinomas present reduced HES1 levels and, interestingly, reduced phosphorylated ERK without changes in phosphorylated MEK. Mechanistically, we show that HES1 directly binds and represses the promoter of *DUSP1*, encoding a dual phosphatase active against phospho-ERK. Accordingly, GSI treatment upregulates DUSP1 and decreases phospho-ERK. These data provide proof for the *in vivo* therapeutic potential of γ-secretase inhibitors in primary NSCLCs.

Keywords

γ-secretase; NOTCH; KRAS; lung cancer; chemotherapy

[*] *Correspondence to*:amaraver@cnio.es, mserrano@cnio.es.

ACCESSION NUMBERS

Microarray data were deposited in NCBI's Gene Expression Omnibus: accession number GSE38054.

SUPPLEMENTAL INFORMATION

Supplemental Information includes seven figures, one table, and Supplemental Experimental Procedures and can be found with this article online.

Europe PMC Funders Author Manuscripts

INTRODUCTION

Lung cancer is the leading cause of cancer-related deaths in the world. A major challenge in treating lung cancer is to find novel therapeutic targets that could complement current chemotherapy.

The Notch pathway is highly complex and regulates among other processes embryonic development, cell fate decisions and tissue homeostasis, and it has been implicated in a variety of human diseases including cancer (Chiba, 2006; Demarest et al., 2008; Ferrando, 2009; Hass et al., 2009; Roy et al., 2007). Briefly, this pathway involves a total of five activatory ligands, four NOTCH receptors, sequential proteolytic processing of the ligand-bound receptors to generate active *N*otch *i*ntra*c*ellular *d*omains (NICDs), and formation of DNA binding complexes with a number of DNA binding partners, being RBPJ the most important and the one that defines the so-called “canonical” Notch pathway (Chiba, 2006; Demarest et al., 2008; Ferrando, 2009; Heitzler, 2010; Roy et al., 2007). In turn, NICD-containing DNA bound complexes activate the expression of a number of effectors, including the transcriptional repressor HES1 (Sang et al., 2010).

The γ-secretase complex is essential for the Notch pathway because it is responsible for the activation of NOTCH receptors by proteolytic cleaveage (Hass et al., 2009). This complex is formed by the assembly of four protein subunits, namely, a presenilin subunit (PSEN1 or PSEN2), nicastrin (NCSTN), APH1 and PSNEN (Fraering, 2007). The proteolytic activity of the γ-secretase complex resides within the presenilin subunit although each of the four subunits is essential for the formation of a functional γ-secretase complex (Fraering, 2007). In this regard, we have recently demonstrated that combined deletion of the two presenilin genes *Psen1* and *Psen2* results in ablation of NOTCH1 activation in T-cells (Maraver et al., 2007). Additionally, small molecule inhibitors targeting the γ-secretase complex (known as GSIs for *γ*-*s*ecretase *i*nhibitors) have been developed (Wolfe, 2009) and phenocopy Notch pathway inhibition in mouse models (van Es et al., 2005; Wong et al., 2004).

The oncogenic role of the Notch pathway is well established in *T*-cell *a*cute *l*ymphoblastic *l*eukemias (T-ALL), where *NOTCH1* is oncogenically mutated in about 60% of leukemias (Ferrando, 2009). Previous investigators have reported a number of alterations in the Notch pathway in human *n*on-*s*mall *c*ell *l*ung *c*arcinomas (NSCLCs), including NOTCH3 overexpression (Haruki et al., 2005), loss of expression of NUMB (Westhoff et al., 2009), a negative regulator of the Notch pathway, and activating mutations in *NOTCH1* (Westhoff et al., 2009). Previous reports have also demonstrated that GSIs induce apoptosis in human lung cancer cells grown *in vitro* (Chen et al., 2007; Eliasz et al., 2010; Westhoff et al., 2009) and slow the growth of subcutaneous xenografts formed by human lung cancer cells (Konishi et al., 2007; Luistro et al., 2009; Paris et al., 2005). However, little is known about the activity of GSIs on primary autochthonous NSCLCs in their natural environment, or about the mechanisms by which GSIs could exert their antitumoral effect on NSCLCs.

In mice, inducible genetic activation of a latent *Kras* oncogenic allele in the lung initiates a stepwise tumorigenic process that culminates in NSCLCs highly similar to those in humans, sharing a common histology (Guerra et al., 2003; Jackson et al., 2001) and a common transcriptional profile (Sweet-Cordero et al., 2005). Here, we have used this mouse model to analyze the effect of the Notch pathway in the development of NSCLCs.

RESULTS

The Notch pathway is hyperactive in murine *Kras*^{G12V}-driven NSCLC

The Notch pathway is hyperactive in a subset of human non-small cell lung carcinomas (NSCLCs) (Westhoff et al., 2009). Based on this, we wanted to know if this was the case in murine *Kras*^{G12V}-driven adenocarcinomas, which is a frequent type of NSCLCs (Guerra et al., 2003). All the analyzed murine NSCLCs presented significantly higher levels of Notch1 intracellular domain (NICD) and Hes1 compared to normal lung (Figure 1A). To evaluate the levels of γ-secretase, we measured the abundance of the active forms of presenilin 1 (PSEN1) and nicastrin (NCSTN). In the case of PSEN1, assembly into the γ-secretase complex is associated to a proteolytic cleavage (Fraering, 2007). We observed higher levels of the carboxy-terminal fragment of PSEN1 (PSEN1-CTF) in murine NSCLCs compared to normal lung (Figure 1A), while the levels of *Psen1* mRNA were unchanged (Figure S1A). These results agree with a previous observation in human fibroblasts cultured *in vitro* where ectopic overexpression of oncogenic *HRAS* was found to increase PSEN1 protein levels without affecting its mRNA levels (Weijzen et al., 2002). In the case of NCSTN, its assembly into the γ-secretase complex is associated to glycosylation and a slower elecretrophoretic mobility (Edbauer et al., 2002). As it was the case of PSEN1, we also observed higher levels of mature NCSTN in murine NSCLCs (Figure S1B). These observations indicate higher levels of functional γ-secretase complex in murine *Kras*^{G12V}-driven NSCLCs.

To define the kinetics of Notch pathway activation during lung tumorigenesis, we tested the expression of HES1 by immunohistochemistry in murine lesions at different stages, from grade 1 to 4 (grades 1 to 3 corresponding to adenomas and grade 4 to adenocarcinomas) (Jackson et al., 2005). Interestingly, we observed a direct association between tumor grade and HES1 nuclear signal, which reached its maximum in grade 4 (adenocarcinomas) lesions (Figures 1B and 1C; Figure S1C). As an internal control, we also observed strong nuclear expression of HES1 in murine bronchioles (Collins et al., 2004; Ito et al., 2000; Morimoto et al.; Tsao et al., 2009) (Figure S1C). Finally, we found lower levels of expression of *Numb* mRNA (Figure 1D), a negative regulator of the Notch pathway whose expression is also diminished in human NSCLC (Westhoff et al., 2009). Together, these data indicate that murine *Kras*^{G12V}-driven NSCLCs faithfully recapitulate the activation of the Notch pathway reported in human NSCLCs and validates this mouse lung cancer model for analyzing therapeutic strategies and mechanisms related to the Notch pathway.

The γ-secretase complex is needed for *Kras*^{G12V}-driven NSCLC

To evaluate the relevance of the Notch pathway in lung tumorigenesis, we combined a Cre-inducible *Kras*^{G12V} oncogenic allele (*Kras*^{LSLG12Vgeo}) (Guerra et al., 2003) and *Psen1*$^{f/f}$;*Psen2*$^{-/-}$ alleles (*i.e. Psen1* flanked by *loxP* sites excisable by Cre recombinase, and *Psen2* null) (Saura et al., 2004), thus generating compound *Kras*$^{+/LSLG12Vgeo}$;*Psen1*$^{f/f}$;*Psen2*$^{-/-}$ animals. These mice were treated with intra-tracheal delivery of adeno-Cre (for brevity, the resulting lungs are referred to here as *Kras V12/PSKO*). Control mice *Kras*$^{+/LSLG12Vgeo}$;*Psen1*$^{+/+}$;*Psen2*$^{+/+}$ were derived from the same set of crosses as the *Kras*$^{+/LSLG12Vgeo}$;*Psen1*$^{f/f}$;*Psen2*$^{-/-}$ mice and, for brevity, we refer to the adeno-Cre treated lungs as *Kras V12/WT* lungs. Mice were sacrificed between 5.5 and 7.5 months post-adeno-Cre delivery and lung tumors were graded and quantified (Figure 2A). Most tumors in control *Kras V12/WT* lungs had progressed to grades 3 and 4, while, in the case of *Kras V12/PSKO* lungs, there was no progression beyond grade 1 (Figure 2A). We also measured the percentage of animals with at least one grade 4 tumor (*i.e.* adenocarcinoma). Importantly, while 44% of *Kras V12/WT* lungs presented adenocarcinomas, none of the *Kras V12/PSKO* lungs developed NSCLCs (Figure 2B).

The canonical Notch pathway is needed for *Kras*^{G12V}-driven NSCLC

After having established the importance of the γ-secretase complex for the generation of *Kras*^{G12V}-driven NSCLC, we wanted to test directly the implication of the canonical Notch pathway. For this, we generated compound mice carrying the Cre-inducible *Kras*^{G12V} oncogenic allele in combination with a floxed allele of *Rbpj* (*Rbpj*$^{f/f}$) (Tanigaki et al., 2002). These mice, together with their corresponding controls, were treated with intra-tracheal delivery of adeno-Cre (for brevity, *Kras V12/RbpjKO* or *Kras V12/WT*, respectively). It should be noted that in this experiment the batch of adeno-Cre was more active than in the previous experiment (see Experimental Procedures), thus yielding a higher number of tumors per mouse. As it happened in *Kras V12/PSKO* mice, in the case of *Kras V12/RbpjKO* mice, grade 4 tumors (adenocarcinomas) were absent 5.5-7.5 months post-adeno-Cre delivery (Figures 3A and 3B). We wondered whether the grade 3 tumors present in *Kras V12/RbpjKO* mice had actually deleted the *Rbpj* gene or, alternatively, were non-deleted *Rbpj*-floxed tumors ("escapers"). For this, we microdissected grade 3 tumors (n=3) and we observed that all of them were "escapers" (Figure S2). Taking together, our genetic analyses indicate that the Notch pathway is essential for NSCLC formation driven by *Kras*^{G12V}.

Pharmacological inhibition of γ-secretase arrests *Kras*^{G12V}-driven NSCLCs

Having demonstrated that γ-secretase is highly relevant for lung tumorigenesis, and that the Notch pathway is strongly active in lung cancer, we set out a preclinical assay to test the impact of γ-secretase inhibition in primary NSCLCs. Previous reports have demonstrated that small molecule inhibitors of the γ-secretase pathway (generally known as GSIs) induce apoptosis in lung cancer cells grown *in vitro* (Chen et al., 2007; Eliasz et al., 2010; Westhoff et al., 2009) and slow the growth of subcutaneous xenografts formed by lung cancer cells (Konishi et al., 2007; Luistro et al., 2009; Paris et al., 2005). However, nothing is known about the impact of GSIs on autochthonous primary NSCLCs, *i.e.* in their natural microenvironment. For this, we took advantage of compound LSN-411575 (Wong et al., 2004). This compound has been well validated in rodents (Best et al., 2005; Wong et al., 2004) and it is among the most potent GSIs (Wolfe, 2009). To test the therapeutic potential of LSN-411575, we used mice carrying the above-mentioned Cre-inducible *Kras*^{G12V} oncogenic allele (*Kras*^{LSLG12Vgeo}) together with a tamoxifen-inducible Cre systemically expressed under the RNA polymerase II promoter (Guerra et al., 2003). These mice develop a mixture of lung adenomas (grades 1 to 3) and adenocarcinomas (grade 4) after induction with tamoxifen. After 6-8 months of tamoxifen induction, we analyzed changes in tumor size and tumor metabolism by X-ray *C*omputed *T*omography (CT) and by *P*ositron *E*mission *T*omography (PET), respectively. Tumors above 0.5 mm diameter were detectable by CT, but only those of grade 4 (*i.e.* adenocarcinomas) were PET-positive (Figures S3A-S3C). Again, this recapitulates the human pathology where only malignant tumors are PET-positive (Fischer et al., 2001; Gould et al., 2001). Mice carrying *Kras*^{G12V}-driven tumors were periodically PET/CT-scanned and those carrying at least one PET-positive tumor were randomly allocated into two groups that were treated daily by gavage with vehicle during 15 days or with 3 mg/kg of LSN-411575 during 15 days or 22 days.

Previous investigators have reported deleterious side effects when using GSIs, especially in the gut (van Es et al., 2005; Wong et al., 2004). In the case of LSN-411575, it has been reported that 10 mg/kg during 15 days produces toxicity in the intestine and mice lose weight, while 1 mg/kg has no detectable effects and animals do not lose weight (Wong et al., 2004). In our case, using 3 mg/kg, mice retained their normal weight after 15 days of treatment, suggesting the absence of deleterious side effects (Figure S3D).

We obtained PET/CT scans of the same mice before and after 15 or 22 days of treatment (Figure 4A). Quantification of the size of the tumors by CT (regardless of whether they are PET-positive or PET-negative) revealed that vehicle-treated tumors increased in size (3.7×-fold) after 15 days, while LSN-411575-treated ones grew significantly less than vehicle-treated controls (1.7×-fold after 15 days and 1.2×-fold after 22 days) (Figure 4B). It is important to note, that some of the animals presented atelectasis, which prevents detection by CT. Given the fact that CT cannot discriminate between non-malignant and malignant tumors, we selectively focused on the response of PET-positive tumors (*i.e.* adenocarcinomas) and quantified their total FDG (^{18}F-fluor-deoxyglucose) uptake pre- and post-treatment. In the case of vehicle-treated mice, PET-positive tumors increased their total FDG uptake an average of 2.2×-fold during the 15 days of treatment (Figure 4C). Importantly, in the case of LSN-411575-treated mice, the average change was 0.7×-fold after 15 days and 1.0×-fold after 22 days (Figure 4C). These results indicate that LSN-411575 has a significant inhibitory effect on the growth of autochthonous murine *Kras*^{G12V}-driven NSCLCs.

Pharmacological inhibition of γ-secretase interferes with ERK phosphorylation in *Kras*^{G12V}-driven NSCLCs

Treated *Kras*^{G12V}-driven NSCLCs (see Figure 4C) were analyzed by immunohistochemistry (samples were obtained 4-8 h after the last treatment). Our first goal was to evaluate whether the GSI treatment had reached its target and, for this, we used the levels of HES1 as a surrogate marker of γ-secretase activity. In accordance with our previous observations (see above Figure 1), vehicle-treated NSCLCs were strongly positive for HES1 (Figure 5A). In contrast to this, LSN-411575-treated (15 days) NSCLCs showed a clear reduction in HES1 levels, confirming that the drug is actually reaching its target within the tumors and at their natural localization (Figure 5A). Also, in agreement with the robust increase in FDG uptake observed during the 15-day interval (Figure 4C), these tumors were highly proliferative (Ki67 staining) and had a low level of apoptosis (activated caspase-3 staining) (Figure 5A). Interestingly, LSN-411575-treated (15 days) NSCLCs presented decreased levels of Ki67-positive cells and a higher frequency of apoptotic cells compared to vehicle-treated tumors (Figure 5A). Of note, these tumors, except for their loss of mitotic cells, retain all their other histological features of grade 4 tumors (characteristically defined by the presence of enlarged pleomorphic nuclei exhibiting a high degree of nuclear atypia and multinucleated giant cells) (Jackson et al., 2005). These observations, strongly suggest that LSN-411575 is arresting cancer growth by inhibiting proliferation and increasing apoptosis.

In an effort to understand the anti-tumoral effect of LSN-411575, we explored a number of key players in lung cancer, such as ERK (Engelman et al., 2008), AKT (Yang et al., 2008), S6K (Liang et al.) and NFκB (Meylan et al., 2009). In the case of AKT (phospho-Ser473-AKT1), S6K (phospho-Thr389-S6K1) and NFκB (nuclear p65), we could not find differences between the staining of NSCLCs treated for 15 days with vehicle or with LSN-411575 (Figure S4A). In contrast to the above, we found a remarkable effect on the activity of ERK. In particular, vehicle-treated NSCLCs were strongly positive for pERK1/pERK2 (phospho-Thr202/Tyr204-ERK1 and phospho-Thr185/Tyr187-ERK2), while LSN-411575-treated NSCLCs were significantly weaker for pERK (Figure 5A). The results obtained by immunohistochemistry were confirmed by immunoblotting of tumor extracts. Specifically, we observed lower levels of HES1 and pERK1/pERK2 in LSN-411575-treated (15 days) NSCLCs compared to the corresponding vehicle-treated tumors (Figure 5B). We wondered whether the lower levels of pERK1/pERK2 were associated to lower levels of its activating kinase MEK, however, the levels of pMEK1/2 (phospho-Ser217/Ser221-MEK1/2) remained similar in vehicle- and LSN-411575-treated NSCLCs (Figure 5B), thus suggesting that the inhibition of pERK exerted by LSN-411575 is independent of MEK

activity. Finally, we wanted to test whether the key observed changes in HES1 and pERK were early events upon LSN-411575 treatment initiation. For this, we treated mice for 4 days with LSN-411575 and, interestingly, the levels of HES1 and pERK in NSCLCs were already lower than in vehicle-treated tumors and similar to tumors treated with the drug for 15 days (Figure 5C). Collectively, these observations indicate that treatment with LSN-411575 arrests *Kras*^{G12V}-driven NSCLCs in association with inhibition of HES1 and ERK phosphorylation.

Inhibition of γ-secretase increases DUSP1 in human and murine oncogenic-*Kras* NSCLCs

Previous investigators have reported that the Notch pathway upregulates pERK levels in *in vitro* cultured cells (Kim et al., 2005; Konishi et al., 2007; Michie et al., 2007). However, the mechanisms involved have remained unexplored. In an effort to understand the link between the Notch pathway and pERK in the context of lung cancer cells, we focused on the human NSCLC cell line H358 which carries an oncogenic *KRAS* allele (*KRAS*^{G12C}) and requires the activity of the oncogene for its viability (Singh et al., 2009). Recapitulating the results obtained in our lung mouse model, H358 cells treated with the γ-secretase inhibitor DAPT (5 μM) also showed lower levels of pERK (Figure 6A). We also explored two other human *KRAS*-mutated NSCLC cell lines, namely, A549 and H23, which carry *KRAS*^{G12S} and *KRAS*^{G12C} alleles, respectively (Blanco et al., 2009), but whose growth is independent of KRAS activity (Singh et al., 2009). Interestingly, these cell lines also showed decreased levels of pERK upon DAPT treatment (Figure S5A), but the magnitude of the effect was not as pronounced as in KRAS-dependent H358 cells.

To get an insight onto the mechanism by which inhibition of the Notch pathway interferes with ERK phosphorylation, we performed RNA microarray analyses to compare GSI-treated and non-treated H358 cells (Table S1). For these assays, we used DAPT, which is a widely used GSI for *in vitro* cultured cells (Wolfe, 2009). As expected, among the genes significantly downregulated by DAPT (FDR $p<0.05$; magnitude $\log_2$ fold change ≤0.5x-fold) we identified *HES1*. Among the genes that showed significant upregulation by DAPT (FDR $p<0.05$; magnitude $\log_2$ fold change ≥0.5x-fold), we noticed the dual specificity phosphatases *DUSP1* and *DUSP6*, which are well-known negative regulators of MAP kinases including ERK (Patterson et al., 2009). Interestingly, *DUSP1* is repressed by the Notch pathway in a NSCLC cell line (Haruki et al., 2005), while we are not aware of a similar link for *DUSP6*. Validation by qRT-PCR confirmed the upregulation of both *DUSP1* and *DUSP6* mRNAs after treatment of H358 cells with DAPT, while *HES1* mRNA levels were downregulated (Figure 6B; Figure S5B). We confirmed that these changes in *HES1* and *DUSP1* mRNA levels correlated with similar changes in the corresponding proteins (Figure 6C). In the case of A549 and H23 cells, both showed a decrease in *HES1* and an upregulation of *DUSP1* upon DAPT treatment, however, only A549 cells presented an upregulation of *DUSP6* (Figure S5B and S5C). In an effort to extrapolate these findings to a different type of Notch-dependent cancer, we performed γ-secretase inhibition of a panel of human T-ALL cell lines and we observed *DUSP1* mRNA upregulation in all of them, albeit with variable magnitude (Figure S5D), while *DUSP6* had an erratic behavior (Figure S5D). These results suggest that the upregulation of *DUSP1* is a general feature of γ-secretase inhibition in cancer.

DUSP1 has been implicated in the dephosphorylation of ERK, JNK and p38 (Patterson et al., 2009). However, treatment with DAPT resulted in reduced levels of pERK (see above Figure 6A) but did not affect the levels of phospho-JNK or phospho-p38 (Figure S5E). We wanted to confirm that DUSP1 is dephosphorylating pERK in our experimental system and for this we ectopically overexpressed a GFP-DUSP1 fusion (Wu et al., 2005) and we measured the levels of pERK by immunofluorescence in the GFP-positive cells. Interestingly, we observed that H358 cells expressing GFP-DUSP1 had very low levels of

pERK upon serum stimulation (10 min), while GFP control cells had high levels of pERK under the same conditions (Figure 6D and 6E). Again, we obtained similar results in A549 and H23 cells (Figure S5F). Conversely, we performed loss of function studies. After testing a total of 12 different RNAi against *DUSP1* (4 siRNAs and 8 shRNAs), we only got a rather modest effect when combining two shRNAs (namely, sh2+sh3) (Figure S5G). Despite the partial decrease in DUSP1 levels, expression of the two shRNAs (sh2+sh3) increased the levels of pERK in transfected H358, compared to a scrambled shRNA (shSC) (Figure 6F). Moreover, expression of sh2+sh3 abolished the inhibitory effect of DAPT on pERK (Figure 6G), suggesting that the effects of DAPT on pERK are mediated by DUSP1. We also wondered whether DAPT treatment affected or not the levels of pMEK in H358 cells. We could not observe changes in pMEK induced by DAPT (Figure S5H), which is in agreement with our previous observations in GSI-treated tumors (Figure 5B). These results support the concept that GSI treatment inhibits KRAS signaling through DUSP1, by decreasing the levels of pERK and without affecting the activity of MEK.

To validate *in vivo* the above data, we compared the levels of *Dusp1* and *Dusp6* mRNAs in primary murine $Kras^{G12V}$-driven NSCLCs treated or not for 15 days with LSN-411575. Importantly, adenocarcinomas from mice treated with LSN-411575, presented increased levels of *Dusp1*/DUSP1 (Figure 6H and 6I) and decreased levels of *Hes1*/HES1 (Figure 5B and 6H) mRNA and protein, compared with vehicle treated adenocarcinomas. In contrast, we could not observe changes in *Dusp6* (Figure S5I). Together, these data establish a tight association between HES1 downregulation and DUSP1 induction upon GSI treatment in cancer.

HES1 directly binds and represses the *DUSP1* promoter

The transcriptional repressor HES1 is a critical mediator of NOTCH1-driven cancer (Wendorff et al., 2010). Based on this and our above data, we hypothesized that HES1 could repress *DUSP1*. To explore this, we began by performing *DUSP1* promoter assays using a luciferase reporter. Interestingly, treatment of H358 cells with DAPT induced the *DUSP1* promoter and this was cancelled when HES1 was co-transfected (Figure 7A). These results further reinforce our previous observations that γ-secretase inhibition upregulates the expression of *DUSP1* and suggest that this could be mediated by the downregulation of HES1. Additionally, the basal activity of the *DUSP1* promoter was decreased by HES1 expression (Figures 7A and 7B). Also, as a marginal note, treatment of cells with a pharmacological MEK inhibitor (PD0325901) decreased the activity of the *DUSP1* promoter (Figure 7B), according to the known role of MEK as a positive regulator of *DUSP1* expression (Brondello et al., 1997), again suggesting that γ-secretase inhibition exerts its actions in a MEK independent manner.

Having observed that HES1 has the ability to repress the *DUSP1* promoter, we asked whether HES1 directly binds to the *DUSP1* promoter. HES1 binds two similar sequence motifs known as class C sites and N-boxes (Iso et al., 2003) and examination of the human and murine *DUSP1/Dusp1* promoters revealed the presence of several putative HES1 binding sites (Figure S6). We tested whether HES1 directly binds to the human *DUSP1* promoter by chromatin immunoprecipitation (ChIP) using two different antibodies against HES1 in H358 cells. Interestingly, HES1 immunoprecipitation with two different antibodies resulted in significant enrichment of two regions of the *DUSP1* promoter compared to a control IgG immunoprecipitation (Figure 7C). In contrast, no enrichment was observed when a *DUSP1* intronic region was amplified or when cells were treated with DAPT (Figure 7C). As a positive control, we used the *DELTEX1* promoter, which is directly repressed by HES1 (Zhang et al., 2010). As expected, binding of HES1 to the *DELTEX1* promoter was observed in the absence of DAPT, but not in its presence (Figure 7C).

We wanted to test the effect of *HES1* inhibition on *DUSP1* levels and ERK phosphorylation. Treatment of H358 cells with a pool of siRNAs targeting *HES1* mRNA (si*HES1*) effectively reduced HES1 mRNA and protein levels (Figures 7D and 7E) and, importantly, this resulted in significant upregulation of DUSP1 mRNA and protein levels (Figures 7D and 7E). We have previously demonstrated that DUSP1 dephosphorylates pERK (Figures 6C and 6D) and, in agreement with this, si*HES1* reduced the levels of phosphorylated ERK (Figures 7E and 7F). Finally, previous reports have shown that GSIs can prevent the growth of human cancer cell lines (Chen et al., 2007; Eliasz et al., 2010; Westhoff et al., 2009) and we wondered whether this could also be the case of si*HES1*. Indeed, cells treated with si*HES1* did have an impaired proliferative capacity (Figure 7G). All together, inhibition of *HES1* in NSCLCs cells recapitulates the effect of DAPT treatment on *DUSP1* expression, ERK phosphorylation and cell proliferation.

High HES1 and low DUSP1 levels are associated with poor clinical outcome in human NSCLCs patients

Previous investigators have reported that subsets of human NSCLCs have hyperactivated the Notch pathway (Haruki et al., 2005; Westhoff et al., 2009) and this correlates with a poor clinical outcome (Westhoff et al., 2009). In the light of our above results, we wanted to extend this to HES1 and to examine its relation with DUSP1. We examined the levels of HES1 in a series of NSCLCs (n=82) observing that tumors with high levels of nuclear HES1 are associated with a shorter overall survival (logrank, p=0.045) (Figure 8A; Figure S7A). Previous investigators have found a positive correlation between DUSP1 levels and survival in human NSCLCs (Vicent et al., 2004). We repeated and confirmed this result in our NSCLCs series where we obtained a positive correlation between DUSP1 cytoplasmic expression and better overall survival (logrank, p=0.048) (Figure 8B; Figure S7A). Moreover, when patients were stratified according to HES1 and DUSP1, those combining high HES1 intensity and low DUSP1 expression had the poorest outcome compared to the other three possible combinations (logrank test, p=0.09) (Figure S7B). Finally, there was a negative correlation between HES1 intensity and DUSP1 expression (correlation coefficient −0.219; Kendall Tau-b test, p=0.07). Collectively, these observations support the relevance of HES1 in human NSCLCs and reinforce the concept that HES1 represses DUSP1.

DISCUSSION

In the present work we have investigated the role of the Notch pathway in the generation and maintenance of primary *Kras*^{G12V}-driven NSCLCs.

It had been previously described that a significant fraction of human NSCLCs present a hyperactive Notch pathway (Haruki et al., 2005; Westhoff et al., 2009), but there was no information about the role of the Notch pathway in the development of NSCLCs. To address this question, we have used a mouse model with a latent *Kras* oncogene that faithfully recapitulates the development of human NSCLCs (Guerra et al., 2003; Jackson et al., 2001; Sweet-Cordero et al., 2005). First, we validated our mouse model by observing that, as in humans, the Notch pathway is hyperactive in murine *Kras*^{G12V}-driven NSCLCs compared to normal lung. This is documented by higher levels of active γ-secretase complex, increased NICD levels (the activated form of NOTCH1), decreased *Numb* mRNA (a negative regulator of the Notch pathway) and increased HES1 protein (a downstream target of Notch). Interestingly, Hes1 protein levels increased in parallel to the degree of malignization, suggesting a requirement of Notch pathway activity during this process. Importantly, genetic elimination of either the γ-secretase complex (upstream of the Notch pathway) or *Rbpj* (encoding the canonical DNA-binding partner of NOTCH receptors) abolished the formation of *Kras*^{G12V}-driven NSCLCs. These results indicate that the generation of NSCLCs by oncogenic *Kras* requires the activation of the Notch pathway.

Based on the above, we hypothesized that Notch activity may be also required for the maintenance of primary *Kras*^{G12V}-driven NSCLCs. Previous reports in this direction have shown that γ-secretase inhibition slows the growth of subcutaneous xenografts formed by lung cancer cells (Konishi et al., 2007; Luistro et al., 2009; Paris et al., 2005). Xenografts, despite their utility, do not recapitulate the microenvironment of the natural primary tumors and this may have a critical impact on therapeutic activity, as it has been elegantly illustrated in the case of pancreatic cancer (Olive et al., 2009). Only a handful of studies have evaluated the efficacy of chemotherapy on primary murine lung tumors (Engelman et al., 2008; Ji et al., 2007; Yang et al., 2008). These studies are largely based on *M*agnetic *R*esonance *I*maging (MRI) or *C*omputed *T*omography (CT), which cannot discriminate non-malignant tumors from malignant ones. Here, in an effort to recapitulate a human clinical setting, we have also evaluated therapeutic responses by *P*ositron *E*mission *T*omography (PET), thus focusing exclusively on malignant tumors. Importantly, mice treated with the pharmacologically active γ-secretase inhibitor LSN-411575 showed a complete blockade of cancer growth. These results demonstrate that GSIs are therapeutically effective in mice for primary autochthonous *Kras*^{G12V}-driven NSCLCs.

Analyses of LSN-411575-treated *Kras*^{G12V}-driven NSCLCs indicated a significant reduction in the levels of HES1 as soon as 4 days after treatment, thus confirming that the GSI reaches its target. In addition, treated NSCLCs presented decreased proliferation and increased apoptosis. Among a number of key candidate proteins that could be affected by GSI treatment, we selectively detected an effect on the phosphorylation of ERK, which was dramatically reduced after treatment. This observation is in accordance with previous data in *in vitro* cultured cells reporting that the Notch pathway upregulates the levels of ERK phosphorylation (Kim et al., 2005; Konishi et al., 2007; Michie et al., 2007). Importantly, the role of ERK phosphorylation in *Kras*-driven NSCLCs has been recently highlighted by the demonstration that ERK activity is essential for *Kras*-driven lung tumorigenesis (Blasco et al., 2011; Feldser et al., 2010; Junttila et al., 2010). Since MEK is the critical kinase responsible for ERK phosphorylation, we also examined the levels of phosphorylated MEK in GSI-treated NSCLCs but, in contrast to phospho-ERK, the levels of phospho-MEK were not affected by the GSI. In summary, we have found that GSI treatment of primary autochthonous *Kras*^{G12V}-driven NSCLCs impinges on the phosphorylation of ERK without affecting MEK activity.

To dissect the mechanism linking γ-secretase inhibition with dephosphorylation of ERK, we analyzed the transcriptional changes induced by GSI. In particular, we used a human NSCLC cell line, H358, which is addicted to oncogenic *KRAS* (Singh et al., 2009). These cells, as we show here, dephosphorylate ERK in response to GSI treatment, without affecting phospho-MEK, thus recapitulating the behavior of primary *Kras*^{G12V}-driven NSCLCs. Among the set of genes whose expression was induced by GSI treatment, we focused our attention on the dual specificity phosphatase DUSP1 because previous data in human NSCLCs cells indicate that this phosphatase is regulated by the Notch pathway (Haruki et al., 2005) and it dephosphorylates ERK (Lin et al., 2003; Patterson et al., 2009). Indeed, we have confirmed with both gain and loss of function experiments the concept that DUSP1 affects ERK phosphorylation in human H358 cells. Moreover, the induction of *DUSP1* after GSI treatment was confirmed in another two human NSCLC cell lines and in six human T-ALL cell lines, thus giving more general validity to our findings. Finally, we observed *Dusp1* upregulation in GSI-treated murine primary *Kras*^{G12V}-driven NSCLCs. Therefore, the observed association between GSI treatment and *DUSP1* upregulation occurs in the context of primary NSCLCs and could explain the reduction in ERK phosphorylation upon GSI treatment.

HES1 is a well-known transcriptional repressor of multiples genes (Iso et al., 2003; Sang et al., 2010), including genes relevant for T-ALL such as *PTEN* (Palomero et al., 2007) and *CYLD* (Espinosa et al., 2010), thus activating AKT and NFκB, respectively. Even more, it has been recently demonstrated that HES1 plays a critical role in the maintenance of NOTCH1-driven murine T-ALL (Wendorff et al., 2010). Based on our observation that HES1 levels increase in association with malignization and decrease upon GSI treatment of $Kras^{G12V}$-driven NSCLCs, we hypothesized that GSI-induced dephosphorylation of ERK could be mediated by HES1-mediated repression of *DUSP1*. Indeed, luciferase reporter assays supported the concept that HES1 is a negative regulator of *DUSP1*. Furthermore, chromatin immunoprecipitation showed that HES1 directly binds and represses *DUSP1*, and importantly, this can be reverted by GSI treatment. Finally, treatment of H358 cells with si*HES1* promoted a phenotype very similar to GSI treatment in terms of ERK phosphorylation, *DUSP1* upregulation and cell growth arrest.

We finally checked the status of HES1 and DUSP1 in primary human NSCLCs. We found that low DUSP1 is associated with poor survival, which is in agreement with previous data (Vicent et al., 2004). In support of our proposed mechanism, we found that high HES1 levels are also associated with poor survival. Moreover, we also observed a suggestive negative correlation between HES1 intensity and DUSP1 expression. These observations support the relevance of HES1 in human NSCLCs and reinforce the concept that HES1 represses DUSP1.

Collectively, our observations establish a direct causal link between γ-secretase inhibition, HES1 downregulation, *DUSP1* derepression and ERK dephosphorylation (Figure 8C). As mentioned above, high ERK activity is crucial for the development of *Kras*-driven NSCLCs (Blasco et al., 2011; Feldser et al., 2010; Junttila et al., 2010) and, in this regard, we propose that our observed requirement of the Notch pathway for NSCLCs formation is related to the capacity of HES1 to increase ERK activity through repression of *Dusp1*. Despite our current data pointing to HES1 and DUSP1 as relevant mediators of the effects of GSI treatment on the KRAS signaling pathway, we cannot exclude the possibility that other members of the HES1 family or DUSP1 family, or other unrelated mechanisms, could also participate in mediating the effects of GSI treatment.

The results presented in this work strengthen the potential therapeutic benefits of targeting γ-secretase in NSCLC. We show that GSI treatment inhibits ERK without affecting MEK and, hence, we envision a synergistic effect of MEK inhibitors and GSIs on *KRAS*-driven NSCLCs. Importantly, GSIs have been shown to be pharmacologically active in humans (Bateman et al., 2009) and have been tested in clinical trials for Alzheimer's disease (Fleisher et al., 2008; Panza et al., 2009; Wolfe, 2009), which could facilitate the evaluation of these compounds for the treatment of human lung cancer, the leading cause of cancer-related deaths in the world.

EXPERIMENTAL PROCEDURES

Mice

Mice were generated by crossing $Kras^{+/LSLG12Vgeo}$ (Guerra et al., 2003) to $Psen1^{f/f};Psen2^{-/-}$ mice (Saura et al., 2004) or $Rbpj^{f/f}$ (Tanigaki et al., 2002) mice. All animal procedures were performed according to protocols approved by the CNIO-ISCIII Ethics Committee for Research and Animal Welfare (CEIyBA).

DNA, RNA and protein analyses

PCR primers are detailed in Supplemental Experimental Procedures, as well as, antibodies and other standard molecular biology methods.

Micro-PET/CT

Imaging was done essentially as described by us elsewhere (Mulero et al., 2011). See summary in Supplemental Experimental Procedures.

Treatment with LSN-411575

The compound was kindly provided by Eli Lilly & Co (Indianapolis, IN) formulated in 1% carboxymethyl cellulose (CMC), 0.25% Tween 80. The compound was given orally by gavage, early in the morning, at a dose of 3 mg/kg/day during the indicated number of days. Control mice were treated with the vehicle following identical procedure. On the last day of treatment, PET was performed within 2-6 hrs after gavage (vehicle- and compound-treated mice were in alternate order for the analysis). Mice were sacrificed (within 4-8 hrs after gavage) and samples were obtained for pathological and immunohistochemical analyses.

Cellular treatments

H358 human NSCLCs cells were purchased from ATCC. Cells were treated with 5 μM DAPT (Calbiochem) for 36 h in the presence of serum. After this, cells were serum starved for 12 h in the presence of DAPT or vehicle, as corresponding. When noted, cells were serum stimulated for the indicated time. For additional details, see Supplemental Experimental Procedures.

Human samples

Primary lung tumors were collected and handled anonymously at collaborating institutions (Instituto Angel H. Roffo and Hospital Britanico) after approval by their Institutional Review Boards (IRB) and following standard ethical and legal protection guidelines of human subjects, including informed consent.

Statistical Analysis

Unless otherwise specified, data are presented as mean ± S.E.M. Student's t test was carried out to assess the significance of expression levels both in qRT-PCR or IHC. Student's t test was also used to determine the differences among groups for changes in size of tumors or animal weight. Associations of protein expression patterns in human TMA of HES1 and DUSP1 were evaluated using the Kendall tau test. Survival curves were tested by logrank test.

Supplementary Material

Refer to Web version on PubMed Central for supplementary material.

Acknowledgments

We are grateful to Mariano Barbacid (CNIO, Madrid) for kindly providing us with inducible KrasG12V mice, Eli Lilly & Co. (Indianapolis, IN) for their generous provision of LSN-411575, Andrew Clark (Imperial College London) for sharing the DUSP1 luciferase reporter, Anton Bennett (Yale University) for sharing the GFP-DUSP1 construct, Francisco Rodríguez (National Center of Biotechnology, Madrid) for help with the adenoviruses, Ramon Diaz-Uriarte (CNIO) for help with statistical analyses, Jose L. de la Pompa (CNIC) for advise, and Daniel Muñoz (CNIO) for critical reading of the manuscript. We would like to thank all the members of our clinical collaborators at the Angel H. Roffo and Hospital Britanico (Buenos Aires, Argentina) involved in this study for their support in facilitating the tumor specimens as well as their corresponding clinical follow-up. A.M. is recipient of a postdoctoral contract of the "Miguel Servet" Program of the Spanish Ministry of Science. Work in the laboratory of M.S. is funded by the CNIO and by grants from the Spanish Ministry of Science (SAF and CONSOLIDER), the European Research Council (ERC Advanced Grant), and the "Marcelino Botin" Foundation. The funders had no role in study design, data collection and analysis, decision to publish, or preparation of the manuscript. A.M. designed and performed most of the experiments, contributed to data analysis, discussion and writing the manuscript; P.J.F.-M. and D.H. performed some experiments and contributed to data analysis; M.M.-M. performed

all the animal manipulations; M.C. performed the murine immunohistochemical and pathological analyses; F.M. performed all the imaging analysis by microPET/CT; D.M. quantified the confocal microscopy; J.S. provided supervision and the mouse model with inducible deletion of γ-secretase; M.S.-Cespedes. and M.S.-Carbayo provided the human samples and performed their immunohistochemical and pathological analyses; T.P. and A.F. gave advise and participated in the design of the study; M.S. designed and supervised the study, secured funding, analyzed the data, and wrote the manuscript. All authors discussed the results and commented on the manuscript. The authors declare no competing financial interests with this paper.

REFERENCES

Bateman RJ, Siemers ER, Mawuenyega KG, Wen G, Browning KR, Sigurdson WC, Yarasheski KE, Friedrich SW, Demattos RB, May PC, et al. A gamma-secretase inhibitor decreases amyloid-beta production in the central nervous system. Ann Neurol. 2009; 66:48–54. [PubMed: 19360898]

Best JD, Jay MT, Otu F, Ma J, Nadin A, Ellis S, Lewis HD, Pattison C, Reilly M, Harrison T, et al. Quantitative measurement of changes in amyloid-beta(40) in the rat brain and cerebrospinal fluid following treatment with the gamma-secretase inhibitor LY-411575 [N2-[(2S)-2-(3,5-difluorophenyl)-2-hydroxyethanoyl]-N1-[(7S)-5-methyl-6-ox o-6,7-dihydro-5H-dibenzo[b,d]azepin-7-yl]-L-alaninamide]. J Pharmacol Exp Ther. 2005; 313:902–908. [PubMed: 15743924]

Blanco R, Iwakawa R, Tang M, Kohno T, Angulo B, Pio R, Montuenga LM, Minna JD, Yokota J, Sanchez-Cespedes M. A gene-alteration profile of human lung cancer cell lines. Hum Mutat. 2009; 30:1199–1206. [PubMed: 19472407]

Blasco RB, Francoz S, Santamaria D, Canamero M, Dubus P, Charron J, Baccarini M, Barbacid M. c-Raf, but not B-Raf, is essential for development of K-Ras oncogene-driven non-small cell lung carcinoma. Cancer Cell. 2011; 19:652–663. [PubMed: 21514245]

Brondello JM, Brunet A, Pouyssegur J, McKenzie FR. The dual specificity mitogen-activated protein kinase phosphatase-1 and -2 are induced by the p42/p44MAPK cascade. J Biol Chem. 1997; 272:1368–1376. [PubMed: 8995446]

Chen Y, De Marco MA, Graziani I, Gazdar AF, Strack PR, Miele L, Bocchetta M. Oxygen concentration determines the biological effects of NOTCH-1 signaling in adenocarcinoma of the lung. Cancer Res. 2007; 67:7954–7959. [PubMed: 17804701]

Chiba S. Notch signaling in stem cell systems. Stem Cells. 2006; 24:2437–2447. [PubMed: 16888285]

Collins BJ, Kleeberger W, Ball DW. Notch in lung development and lung cancer. Semin Cancer Biol. 2004; 14:357–364. [PubMed: 15288261]

Demarest RM, Ratti F, Capobianco AJ. It's T-ALL about Notch. Oncogene. 2008; 27:5082–5091. [PubMed: 18758476]

Edbauer D, Winkler E, Haass C, Steiner H. Presenilin and nicastrin regulate each other and determine amyloid beta-peptide production via complex formation. Proc Natl Acad Sci U S A. 2002; 99:8666–8671. [PubMed: 12048259]

Eliasz S, Liang S, Chen Y, De Marco MA, Machek O, Skucha S, Miele L, Bocchetta M. Notch-1 stimulates survival of lung adenocarcinoma cells during hypoxia by activating the IGF-1R pathway. Oncogene. 2010; 29:2488–2498. [PubMed: 20154720]

Engelman JA, Chen L, Tan X, Crosby K, Guimaraes AR, Upadhyay R, Maira M, McNamara K, Perera SA, Song Y, et al. Effective use of PI3K and MEK inhibitors to treat mutant Kras G12D and PIK3CA H1047R murine lung cancers. Nat Med. 2008; 14:1351–1356. [PubMed: 19029981]

Espinosa L, Cathelin S, D'Altri T, Trimarchi T, Statnikov A, Guiu J, Rodilla V, Ingles-Esteve J, Nomdedeu J, Bellosillo B, et al. The Notch/Hes1 pathway sustains NF-kappaB activation through CYLD repression in T cell leukemia. Cancer Cell. 2010; 18:268–281. [PubMed: 20832754]

Feldser DM, Kostova KK, Winslow MM, Taylor SE, Cashman C, Whittaker CA, Sanchez-Rivera FJ, Resnick R, Bronson R, Hemann MT, et al. Stage-specific sensitivity to p53 restoration during lung cancer progression. Nature. 2010; 468:572–575. [PubMed: 21107428]

Ferrando AA. The role of NOTCH1 signaling in T-ALL. Hematology Am Soc Hematol Educ Program. 2009:353–361. [PubMed: 20008221]

Fischer BM, Mortensen J, Hojgaard L. Positron emission tomography in the diagnosis and staging of lung cancer: a systematic, quantitative review. Lancet Oncol. 2001; 2:659–666. [PubMed: 11902536]

Fleisher AS, Raman R, Siemers ER, Becerra L, Clark CM, Dean RA, Farlow MR, Galvin JE, Peskind ER, Quinn JF, et al. Phase 2 safety trial targeting amyloid beta production with a gamma-secretase inhibitor in Alzheimer disease. Arch Neurol. 2008; 65:1031–1038. [PubMed: 18695053]

Fraering PC. Structural and Functional Determinants of gamma-Secretase, an Intramembrane Protease Implicated in Alzheimer's Disease. Curr Genomics. 2007; 8:531–549. [PubMed: 19415127]

Gould MK, Maclean CC, Kuschner WG, Rydzak CE, Owens DK. Accuracy of positron emission tomography for diagnosis of pulmonary nodules and mass lesions: a meta-analysis. JAMA. 2001; 285:914–924. [PubMed: 11180735]

Guerra C, Mijimolle N, Dhawahir A, Dubus P, Barradas M, Serrano M, Campuzano V, Barbacid M. Tumor induction by an endogenous K-ras oncogene is highly dependent on cellular context. Cancer Cell. 2003; 4:111–120. [PubMed: 12957286]

Haruki N, Kawaguchi KS, Eichenberger S, Massion PP, Olson S, Gonzalez A, Carbone DP, Dang TP. Dominant-negative Notch3 receptor inhibits mitogen-activated protein kinase pathway and the growth of human lung cancers. Cancer Res. 2005; 65:3555–3561. [PubMed: 15867348]

Hass MR, Sato C, Kopan R, Zhao G. Presenilin: RIP and beyond. Semin Cell Dev Biol. 2009; 20:201–210. [PubMed: 19073272]

Heitzler P. Biodiversity and noncanonical Notch signaling. Curr Top Dev Biol. 2010; 92:457–481. [PubMed: 20816404]

Iso T, Kedes L, Hamamori Y. HES and HERP families: multiple effectors of the Notch signaling pathway. J Cell Physiol. 2003; 194:237–255. [PubMed: 12548545]

Ito T, Udaka N, Yazawa T, Okudela K, Hayashi H, Sudo T, Guillemot F, Kageyama R, Kitamura H. Basic helix-loop-helix transcription factors regulate the neuroendocrine differentiation of fetal mouse pulmonary epithelium. Development. 2000; 127:3913–3921. [PubMed: 10952889]

Jackson EL, Olive KP, Tuveson DA, Bronson R, Crowley D, Brown M, Jacks T. The differential effects of mutant p53 alleles on advanced murine lung cancer. Cancer Res. 2005; 65:10280–10288. [PubMed: 16288016]

Jackson EL, Willis N, Mercer K, Bronson RT, Crowley D, Montoya R, Jacks T, Tuveson DA. Analysis of lung tumor initiation and progression using conditional expression of oncogenic K-ras. Genes Dev. 2001; 15:3243–3248. [PubMed: 11751630]

Ji H, Wang Z, Perera SA, Li D, Liang MC, Zaghlul S, McNamara K, Chen L, Albert M, Sun Y, et al. Mutations in BRAF and KRAS converge on activation of the mitogen-activated protein kinase pathway in lung cancer mouse models. Cancer Res. 2007; 67:4933–4939. [PubMed: 17510423]

Junttila MR, Karnezis AN, Garcia D, Madriles F, Kortlever RM, Rostker F, Brown Swigart L, Pham DM, Seo Y, Evan GI, et al. Selective activation of p53-mediated tumour suppression in high-grade tumours. Nature. 2010; 468:567–571. [PubMed: 21107427]

Kim MY, Park JH, Choi EJ, Park HS. Presenilin acts as a positive regulator of basal level activity of ERK through the Raf-MEK1 signaling pathway. Biochem Biophys Res Commun. 2005; 332:609–613. [PubMed: 15896720]

Konishi J, Kawaguchi KS, Vo H, Haruki N, Gonzalez A, Carbone DP, Dang TP. Gamma-secretase inhibitor prevents Notch3 activation and reduces proliferation in human lung cancers. Cancer Res. 2007; 67:8051–8057. [PubMed: 17804716]

Liang MC, Ma J, Chen L, Kozlowski P, Qin W, Li D, Goto J, Shimamura T, Hayes DN, Meyerson M, et al. TSC1 loss synergizes with KRAS activation in lung cancer development in the mouse and confers rapamycin sensitivity. Oncogene. 29:1588–1597. [PubMed: 19966866]

Lin YW, Chuang SM, Yang JL. ERK1/2 achieves sustained activation by stimulating MAPK phosphatase-1 degradation via the ubiquitin-proteasome pathway. J Biol Chem. 2003; 278:21534–21541. [PubMed: 12676937]

Luistro L, He W, Smith M, Packman K, Vilenchik M, Carvajal D, Roberts J, Cai J, Berkofsky-Fessler W, Hilton H, et al. Preclinical profile of a potent gamma-secretase inhibitor targeting notch signaling with in vivo efficacy and pharmacodynamic properties. Cancer Res. 2009; 69:7672–7680. [PubMed: 19773430]

Maraver A, Tadokoro CE, Badura ML, Shen J, Serrano M, Lafaille JJ. Effect of presenilins in the apoptosis of thymocytes and homeostasis of CD8+ T cells. Blood. 2007; 110:3218–3225. [PubMed: 17626841]

Meylan E, Dooley AL, Feldser DM, Shen L, Turk E, Ouyang C, Jacks T. Requirement for NF-kappaB signalling in a mouse model of lung adenocarcinoma. Nature. 2009; 462:104–107. [PubMed: 19847165]

Michie AM, Chan AC, Ciofani M, Carleton M, Lefebvre JM, He Y, Allman DM, Wiest DL, Zuniga-Pflucker JC, Izon DJ. Constitutive Notch signalling promotes CD4 CD8 thymocyte differentiation in the absence of the pre-TCR complex, by mimicking pre-TCR signals. Int Immunol. 2007; 19:1421–1430. [PubMed: 17981791]

Morimoto M, Liu Z, Cheng HT, Winters N, Bader D, Kopan R. Canonical Notch signaling in the developing lung is required for determination of arterial smooth muscle cells and selection of Clara versus ciliated cell fate. J Cell Sci. 123:213–224. [PubMed: 20048339]

Mulero F, Donate LE, Serrano M. Imaging cancer in mice by PET, CT, and combined PET-CT. Curr Protoc Mouse Biol. 2011; 1:85–103.

Olive KP, Jacobetz MA, Davidson CJ, Gopinathan A, McIntyre D, Honess D, Madhu B, Goldgraben MA, Caldwell ME, Allard D, et al. Inhibition of Hedgehog signaling enhances delivery of chemotherapy in a mouse model of pancreatic cancer. Science. 2009; 324:1457–1461. [PubMed: 19460966]

Palomero T, Sulis ML, Cortina M, Real PJ, Barnes K, Ciofani M, Caparros E, Buteau J, Brown K, Perkins SL, et al. Mutational loss of PTEN induces resistance to NOTCH1 inhibition in T-cell leukemia. Nat Med. 2007; 13:1203–1210. [PubMed: 17873882]

Panza F, Solfrizzi V, Frisardi V, Imbimbo BP, Capurso C, D'Introno A, Colacicco AM, Seripa D, Vendemiale G, Capurso A, et al. Beyond the neurotransmitter-focused approach in treating Alzheimer's disease: drugs targeting beta-amyloid and tau protein. Aging Clin Exp Res. 2009; 21:386–406. [PubMed: 20154508]

Paris D, Quadros A, Patel N, DelleDonne A, Humphrey J, Mullan M. Inhibition of angiogenesis and tumor growth by beta and gamma-secretase inhibitors. Eur J Pharmacol. 2005; 514:1–15. [PubMed: 15878319]

Patterson KI, Brummer T, O'Brien PM, Daly RJ. Dual-specificity phosphatases: critical regulators with diverse cellular targets. Biochem J. 2009; 418:475–489. [PubMed: 19228121]

Roy M, Pear WS, Aster JC. The multifaceted role of Notch in cancer. Curr Opin Genet Dev. 2007; 17:52–59. [PubMed: 17178457]

Sang L, Roberts JM, Coller HA. Hijacking HES1: how tumors co-opt the anti-differentiation strategies of quiescent cells. Trends Mol Med. 2010; 16:17–26. [PubMed: 20022559]

Saura CA, Choi SY, Beglopoulos V, Malkani S, Zhang D, Shankaranarayana Rao BS, Chattarji S, Kelleher RJ 3rd, Kandel ER, Duff K, et al. Loss of presenilin function causes impairments of memory and synaptic plasticity followed by age-dependent neurodegeneration. Neuron. 2004; 42:23–36. [PubMed: 15066262]

Singh A, Greninger P, Rhodes D, Koopman L, Violette S, Bardeesy N, Settleman J. A gene expression signature associated with "K-Ras addiction" reveals regulators of EMT and tumor cell survival. Cancer Cell. 2009; 15:489–500. [PubMed: 19477428]

Sweet-Cordero A, Mukherjee S, Subramanian A, You H, Roix JJ, Ladd-Acosta C, Mesirov J, Golub TR, Jacks T. An oncogenic KRAS2 expression signature identified by cross-species gene-expression analysis. Nat Genet. 2005; 37:48–55. [PubMed: 15608639]

Tanigaki K, Han H, Yamamoto N, Tashiro K, Ikegawa M, Kuroda K, Suzuki A, Nakano T, Honjo T. Notch-RBP-J signaling is involved in cell fate determination of marginal zone B cells. Nat Immunol. 2002; 3:443–450. [PubMed: 11967543]

Tsao PN, Vasconcelos M, Izvolsky KI, Qian J, Lu J, Cardoso WV. Notch signaling controls the balance of ciliated and secretory cell fates in developing airways. Development. 2009; 136:2297–2307. [PubMed: 19502490]

van Es JH, van Gijn ME, Riccio O, van den Born M, Vooijs M, Begthel H, Cozijnsen M, Robine S, Winton DJ, Radtke F, et al. Notch/gamma-secretase inhibition turns proliferative cells in intestinal crypts and adenomas into goblet cells. Nature. 2005; 435:959–963. [PubMed: 15959515]

Vicent S, Garayoa M, Lopez-Picazo JM, Lozano MD, Toledo G, Thunnissen FB, Manzano RG, Montuenga LM. Mitogen-activated protein kinase phosphatase-1 is overexpressed in non-small cell lung cancer and is an independent predictor of outcome in patients. Clin Cancer Res. 2004; 10:3639–3649. [PubMed: 15173070]

Weijzen S, Rizzo P, Braid M, Vaishnav R, Jonkheer SM, Zlobin A, Osborne BA, Gottipati S, Aster JC, Hahn WC, et al. Activation of Notch-1 signaling maintains the neoplastic phenotype in human Ras-transformed cells. Nat Med. 2002; 8:979–986. [PubMed: 12185362]

Wendorff AA, Koch U, Wunderlich FT, Wirth S, Dubey C, Bruning JC, MacDonald HR, Radtke F. Hes1 is a critical but context-dependent mediator of canonical Notch signaling in lymphocyte development and transformation. Immunity. 2010; 33:671–684. [PubMed: 21093323]

Westhoff B, Colaluca IN, D'Ario G, Donzelli M, Tosoni D, Volorio S, Pelosi G, Spaggiari L, Mazzarol G, Viale G, et al. Alterations of the Notch pathway in lung cancer. Proc Natl Acad Sci U S A. 2009; 106:22293–22298. [PubMed: 20007775]

Wolfe MS. gamma-Secretase in biology and medicine. Semin Cell Dev Biol. 2009; 20:219–224. [PubMed: 19162210]

Wong GT, Manfra D, Poulet FM, Zhang Q, Josien H, Bara T, Engstrom L, Pinzon-Ortiz M, Fine JS, Lee HJ, et al. Chronic treatment with the gamma-secretase inhibitor LY-411,575 inhibits beta-amyloid peptide production and alters lymphopoiesis and intestinal cell differentiation. J Biol Chem. 2004; 279:12876–12882. [PubMed: 14709552]

Wu JJ, Zhang L, Bennett AM. The noncatalytic amino terminus of mitogen-activated protein kinase phosphatase 1 directs nuclear targeting and serum response element transcriptional regulation. Mol Cell Biol. 2005; 25:4792–4803. [PubMed: 15899879]

Yang Y, Iwanaga K, Raso MG, Wislez M, Hanna AE, Wieder ED, Molldrem JJ, Wistuba, Powis G, Demayo FJ, et al. Phosphatidylinositol 3-kinase mediates bronchioalveolar stem cell expansion in mouse models of oncogenic K-ras-induced lung cancer. PLoS One. 2008; 3:e2220. [PubMed: 18493606]

Zhang P, Yang Y, Nolo R, Zweidler-McKay PA, Hughes DP. Regulation of NOTCH signaling by reciprocal inhibition of HES1 and Deltex 1 and its role in osteosarcoma invasiveness. Oncogene. 2010; 29:2916–2926. [PubMed: 20208568]

Europe PMC Funders Author Manuscripts

Europe PMC Funders Author Manuscripts

SIGNIFICANCE

NOTCH oncogenic mutations have been found in T-cell leukemias and lung cancer. In T-cell leukemias, oncogenic NOTCH activates AKT and NFκB through HES1-mediated transcriptional repression of *PTEN* and *CYLD*, respectively. Little is known, however, about how the Notch pathway participates in lung cancer. Here, we show that Notch pathway inhibition, either genetically or pharmacologically, hampers primary $Kras^{G12V}$-driven non-small cell lung carcinomas (NSCLCs). We demonstrate that HES1 directly represses the promoter of *DUSP1*, which encodes a dual specificity phosphatase with activity against phospho-ERK. Treatment with GSIs induces *DUSP1* expression and this is associated with loss of ERK phosphorylation, a critical player in NSCLCs. These results validate the potential of GSIs in the treatment of primary NSCLCs.

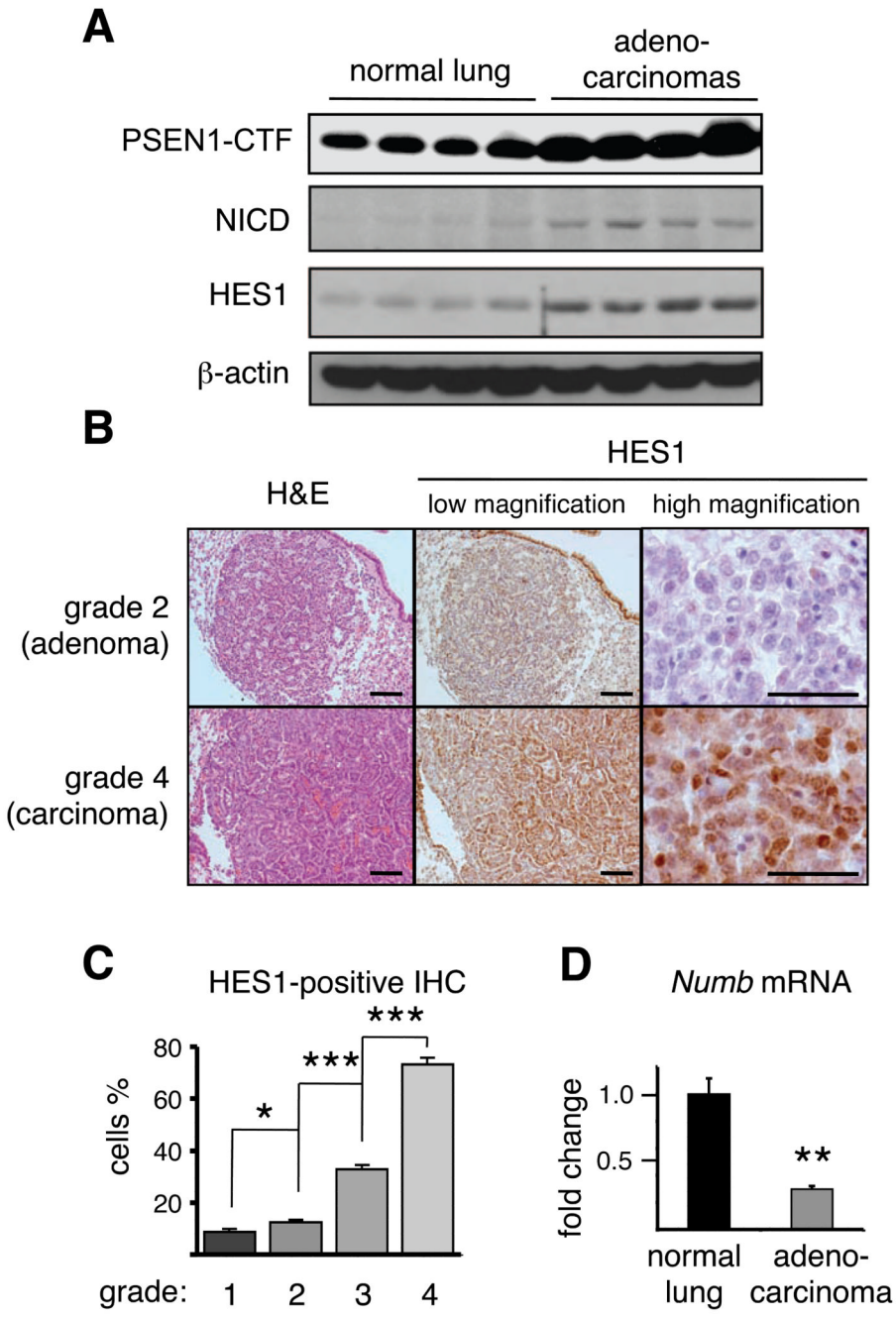

Figure 1. Activity of the Notch pathway in murine *Kras*^{G12V}-driven NSCLC

(A) Analysis of γ-secretase activity by detection of presenilin carboxy-terminal fragment (PSEN1-CTF) or Notch1 activity by detection of NOTCH1 intracellular domain (NICD) and HES by immunobloting ("lung": each lane corresponds to a different control WT mouse; "adenocarcinomas": each lane corresponds to a grade 4 tumor from a different mouse). Bars in the four leftmost panels correspond to 100 μm. Bars in the two rightmost panels correspond to 50 μm.

(B) Detection of HES1 in murine *Kras*^{G12V} lung tumors. Representative examples of grade 2 (adenoma) and grade 4 (adenocarcinoma) tumors stained with (left) H&E and HES1 (middle and right) at low magnification (middle) or high magnification (right).
(C) Quantification of HES1 during lung tumorigenesis. The graph depicts percentage of HES1-positive nuclei (detected by immunohistochemistry as in panel B) within tumors of different grades (n=5 for each tumor grade).
(D) Levels of *Numb* mRNA measured by qRT-PCR from WT mouse lungs (n=4) and grade 4 tumors (n=4).
Values correspond to the average ± SEM. Statistical significance was determined by the two-tailed Student's *t*-test: * $p< 0.05$; ** $p< 0.01$; *** $p<0.001$.
See also Figure S1.

Europe PMC Funders Author Manuscripts

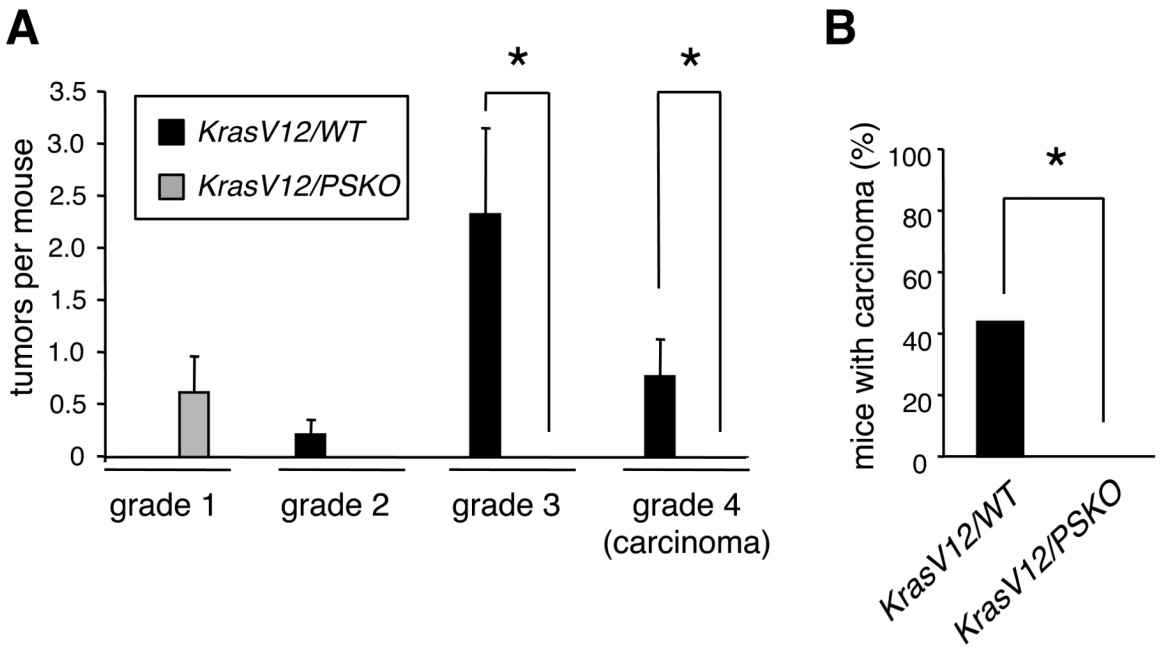

Figure 2. Presenilins 1 and 2 are needed for the generation of *Kras*^{G12V}-driven NSCLC

(A) The graph depicts the number and grade of tumors per animal. Lungs from *KrasV12/WT* and *KrasV12/PSKO* mice were pathologically analyzed 5.5-7.5 months after adeno-Cre delivery. For each genotype, n=9 mice.

(B) Percentage of mice carrying grade 4 (adenocarcinoma) tumors. For each genotype, n=9 mice.

Values correspond to the average ± SEM. Statistical significance was determined by the two-tailed Student's *t*-test (part A) or by the Fisher's exact test (part B): * $p < 0.05$.

Europe PMC Funders Author Manuscripts

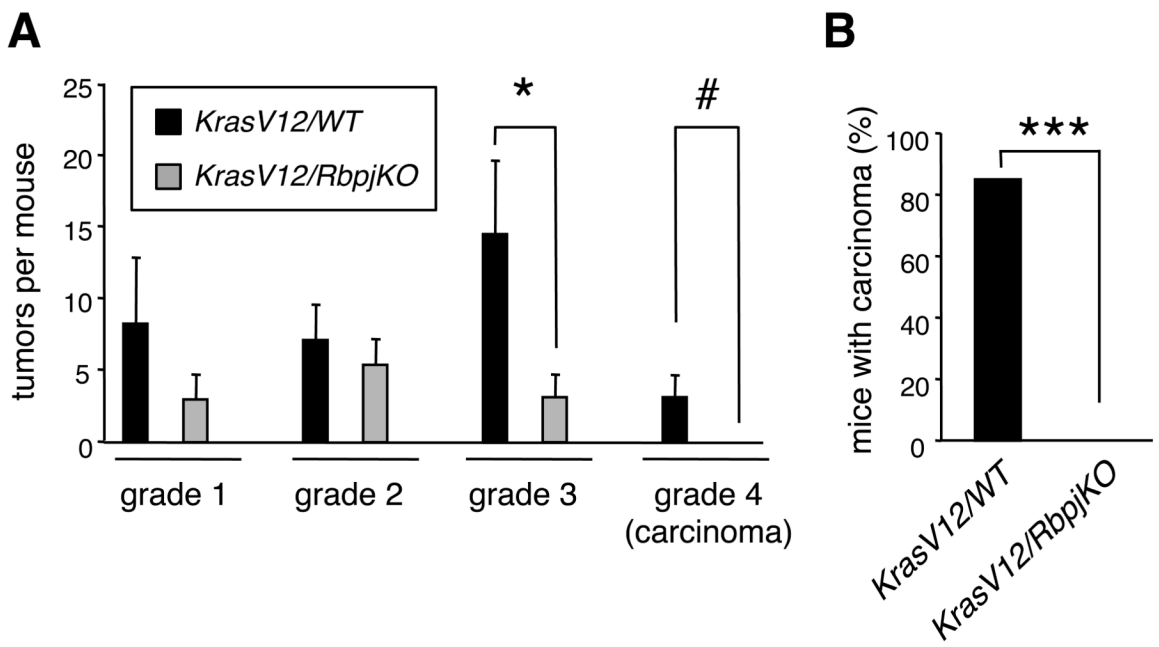

Figure 3. The canonical Notch pathway is needed for the generation of *Kras*^{G12V}-driven NSCLC

(A) The graph depicts the number and grade of tumors per animal. Lungs from *KrasV12/WT* and *KrasV12/RbpjKO* mice were pathologically analyzed 5.5-7.5 months after adeno-Cre delivery. For each genotype, n=7 mice.

(B) Percentage of mice carrying grade 4 (adenocarcinoma) tumors. For each genotype, n=7 mice.

Values correspond to the ± SEM. Statistical significance was determined by the two-tailed Student's *t*-test (part A) or by the Fisher's exact test (part B): # $p< 0.1$; * $p< 0.05$; *** $p<0.001$.

See also Figure S2.

Europe PMC Funders Author Manuscripts

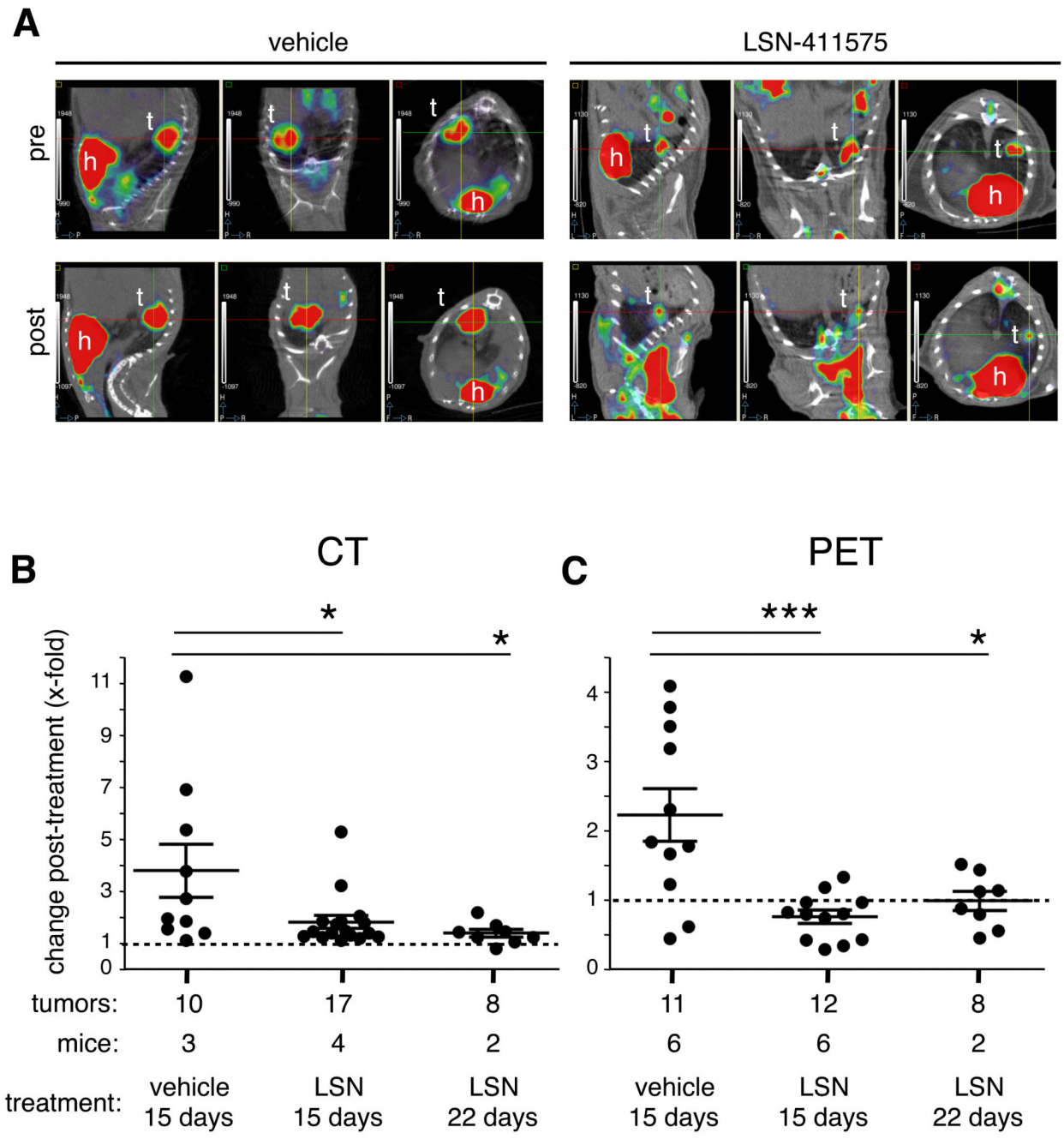

Figure 4. Pharmacological inhibition of γ-secretase arrests *Kras*^{G12V}-driven NSCLCs

(A) Representative examples of PET/CT analyses of a single *Kras*^{G12V} mouse at the beginning (pre) and at the end (post) of 15 days treatment with vehicle (left) or of a single *Kras*^{G12V} mouse treated with LSN-411575 (right). Images correspond to sagittal (left panels), coronal (middle panels) and transverse (right panels) views. The position of the PET-positive tumor (t) and the position of the heart (h) are labeled.

(B) Change in total tumor size detected by CT after 15 days treatment with vehicle or after 15 or 22 days of treatment with LSN-411575.

(C) Change in total ^{18}F-FDG uptake of PET-positive tumors after 15 days treatment with vehicle or after 15 or 22 days of treatment with LSN-411575.
Values correspond to the relative change of each individual tumor from the day before starting the treatment to the last day of treatment. Bars correspond to the average ± SEM. Statistical analysis was performed by the two-tailed Student's *t*-test (shown in the top of the graph). Symbols of statistical significance are: * $p< 0.05$; *** $p<0.001$.
See also Figure S3.

Europe PMC Funders Author Manuscripts

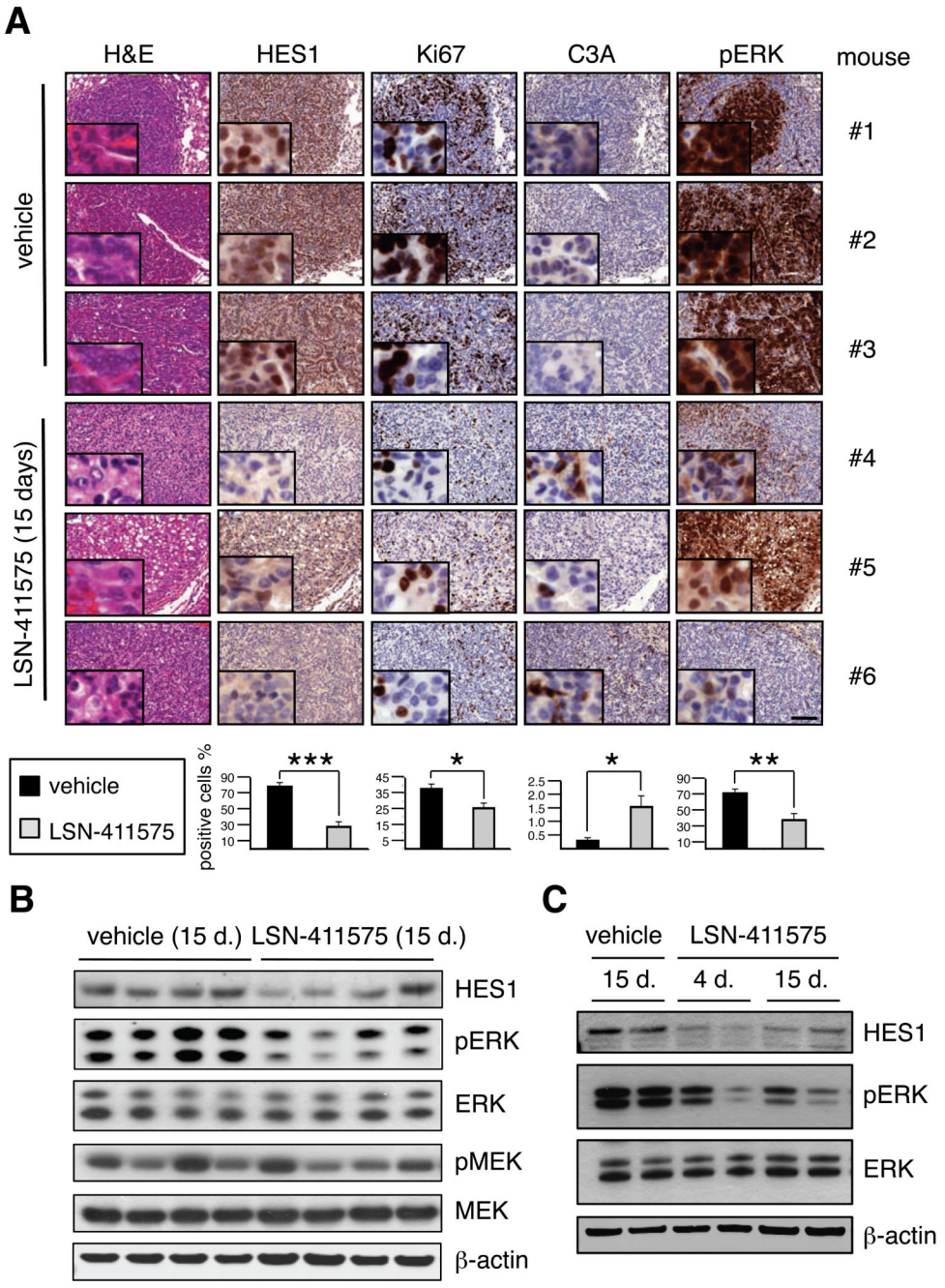

Figure 5. Pharmacological inhibition of γ-secretase diminishes HES1 and pERK in *Kras*^{G12V}-driven NSCLCs

(A) Immunohistochemical analyses of NSCLCs after 15 days treatment with vehicle or LSN-411575. Rows correspond to serial sections of the same tumor. Three examples of vehicle-treated tumors or LSN-411575-treated tumors are shown (each example is from a different mouse). All pictures are at the same magnification. The bar in the lower right panel corresponds to 100 μm. The quantifications shown at the bottom correspond to all the analyzed NSCLCs: vehicle, 11 tumors (n=11) present in 6 mice; LSN-411575, 12 tumors (n=12) present in 6 mice. For each staining, 2 separate fields at 20x magnification were counted and an average of 1500 cells were scored per tumor. Values correspond to the

average ± SEM. Statistical significance was determined by the two-tailed Student's *t*-test. Symbols of statistical significance are: * p< 0.05; ** p<0.01; *** p<0.001.

(B) Immunoblotting of the indicated proteins in PET-positive NSCLCs treated for 15 days with vehicle or LSN-411575. Each lane corresponds to a different tumor from a different mouse.

(C) Immunoblotting of the indicated proteins in PET-positive NSCLCs treated with vehicle or LSN-411575 for the indicated periods of time (4 days or 15 days). Each lane corresponds to a different tumor from a different mouse.

See also Figure S4.

Europe PMC Funders Author Manuscripts

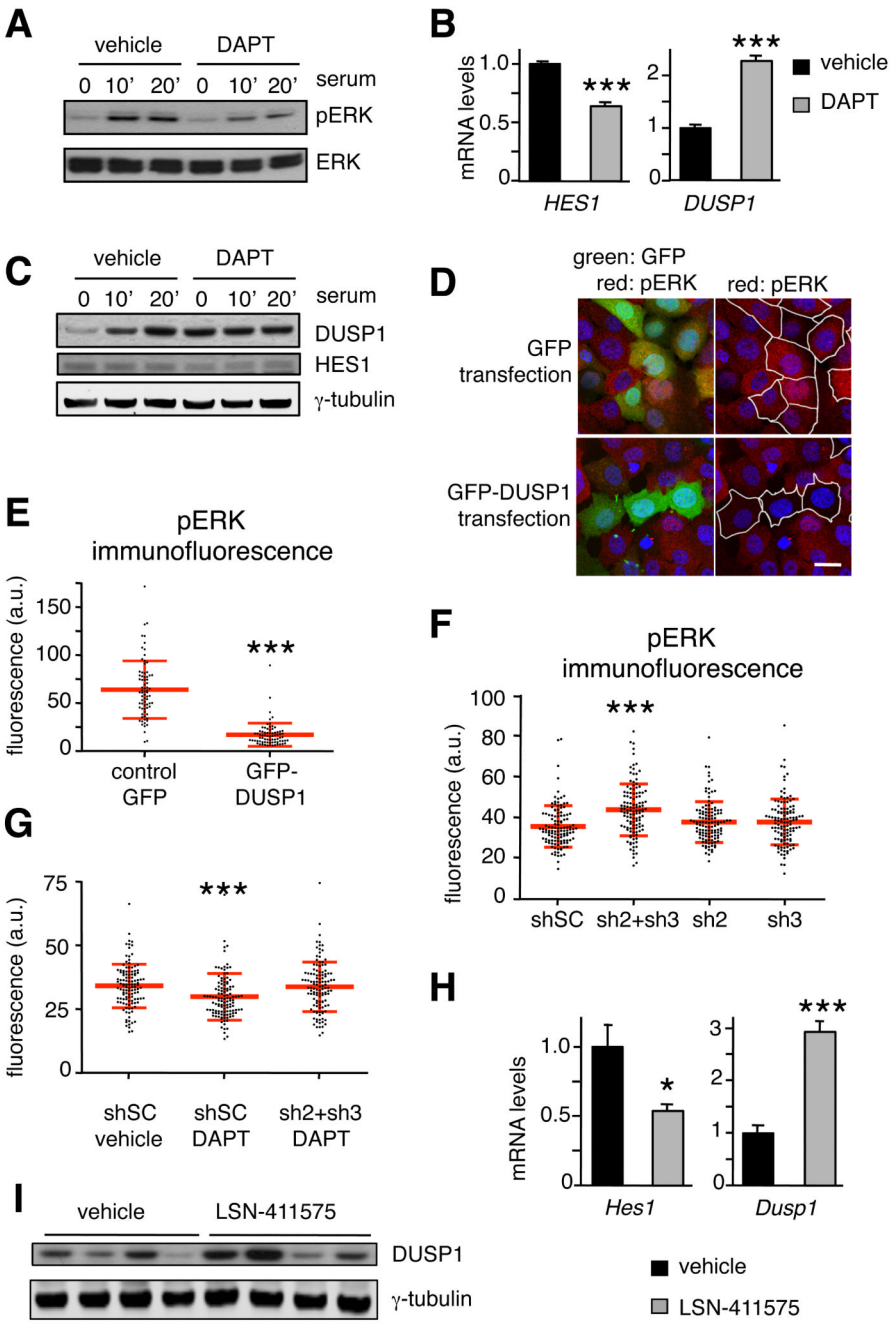

Figure 6. Inhibition of γ-secretase increases *DUSP1* in human and mouse NSCLCs

(A) Analysis of pERK in H358 cells treated with 5 μM DAPT (DAPT) or with vehicle. Cells were treated for 48 h (36 h in the presence of serum and then 12 h in the absence of serum) and then stimulated with serum for the indicated times (in minutes).

(B) Analysis of *DUSP1* and *HES1* expression by qRT-PCR in non-treated (vehicle, n=3) or DAPT treated (5 μM DAPT, n=3) H358 cells. Cells were treated for 48 h (36 h in the presence of serum and then 12 h in the absence of serum). All pictures are at the same magnification. The bar in the lower right panel corresponds to 20 μm.

(C) Analysis of DUSP1 and HES1 in H358 cells treated with 5 μM DAPT (DAPT) or with vehicle. Cells were treated for 48 h (36 h in the presence of serum and then 12 h in the absence of serum) and then stimulated with serum for the indicated times (in minutes).
(**D**) Fluorescence detection of GFP and phospho-ERK in H358 cells transfected with GFP alone or with a GFP-DUSP1 fusion. Cells were starved and serum stimulated for 10 min. GFP-positive cells are marked with a white line.
(E) Quantification of the experiment shown in panel C. GFP-positive cells (n=75) were quantified with an automatic software for each transfection (GFP alone, or GFP-DUSP1).
(F) Fluorescence detection of GFP and quantification of phospho-ERK in H358 cells transfected with pGIPZ scramble (shSC), with pGIPZ anti-DUSP1 shRNAs (sh2, sh3 and sh2+sh3). 36 hours after transfection cells were starved for 12 h and serum stimulated for 10 min. GFP-positive cells (n=120) were quantified with automatic software for each transfection.
(G) Cells were transfected as in panel F and 6 hours after transfection cells were treated with vehicle or with DAPT (5 μM) for 48 h (36 h in the presence of serum and then 12 h in the absence of serum) and then stimulated with serum for 10 minutes. GFP-positive cells (n=120) were quantified with automatic software for each transfection.
(**H**) Analysis of *Hes1* and *Dusp1* expression by qRT-PCR in PET-positive $Kras^{G12V}$-driven NSCLCs treated with LSN-411575 (n=4) or vehicle (n=4) for 15 days.
(I) Immunoblotting of the indicated proteins in PET-positive $Kras^{G12V}$-driven NSCLCs treated for 15 days with vehicle or LSN-411575. Each lane corresponds to a different adenocarcinoma from a different mouse. These adenocarcinomas are the same analyzed in Figure 5B and are loaded in the same order.
Values correspond to the average. Error bars in panels B and H correspond to SEM. Error bars in panels E, F and G correspond to SD. Statistical significance was determined by the two-tailed Student's *t*-test: * $p< 0.05$; *** $p<0.001$.
See also Figure S5.

Europe PMC Funders Author Manuscripts

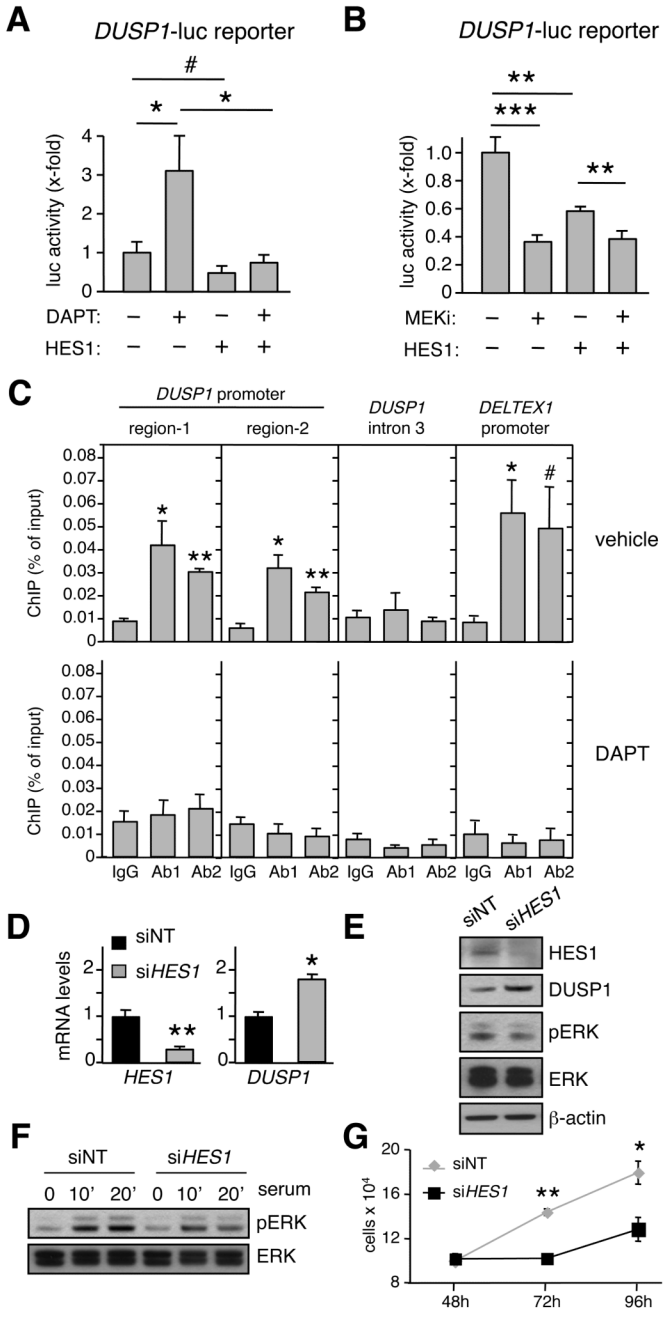

Figure 7. HES1 directly binds and represses the *DUSP1* promoter

(A) Luciferase activity of H358 cells transfected with a *DUSP1*-luc reporter together with a plasmid expressing HES1 or its corresponding empty control. Cells were treated for 48 h with DAPT or its vehicle in the presence of complete medium.

(B) Luciferase activity of H358 cells transfected with a *DUSP1*-luc reporter together with a plasmid expressing HES1 or its corresponding empty control. Cells were treated for 48 h with a MEK inhibitor (PD0325901) or its vehicle in the presence of complete medium.

(C) ChIP analysis of the *DUSP1* promoter using 2 different HES1 antibodies (Ab1, 4H1 Novus Biologicals; Ab2, H140 Santa Cruz) in H358 cells. Two different regions of the

DUSP1 promoter (see Figure S5), an intronic region from *DUSP1* (intron 3), and the promoter of *DELTEX1* were amplified by qPCR. Cells were treated (5 μM DAPT) or not (ETOH) with DAPT for 48 h. Data correspond to three independent biological replicates.
(D) Levels of *HES1* and *DUSP1* expression measured by qRT-PCR in H358 cells treated with si*HES1* (*HES1* siRNA, n=3) or siNT (NT siRNA, n=3) for 48 h (36 h in the presence of serum and then 12 h in the absence of serum).
(E) Protein levels of DUSP1, HES1, pERK and total ERK in H358 cells treated as in panel D.
(F) Phosphorylation of ERK in H358 cells treated with si*HES1* (*HES1* siRNA) or siNT (NT siRNA) for 48 h (36 h in the presence of serum and then 12 h in the absence of serum) and then stimulated with serum for the indicated times (in minutes).
(G) H358 cells were treated with si*HES1* (*HES1* siRNA, n=3) or siNT (NT siRNA, n=3) and cell numbers were counted at the indicated time points after siRNA transfection. Values correspond to the average ± SEM. Statistical significance was determined by the two-tailed Student's *t*-test: # $p<0.1$; * $p< 0.05$; ** $p<0.01$.
See also Figure S6.

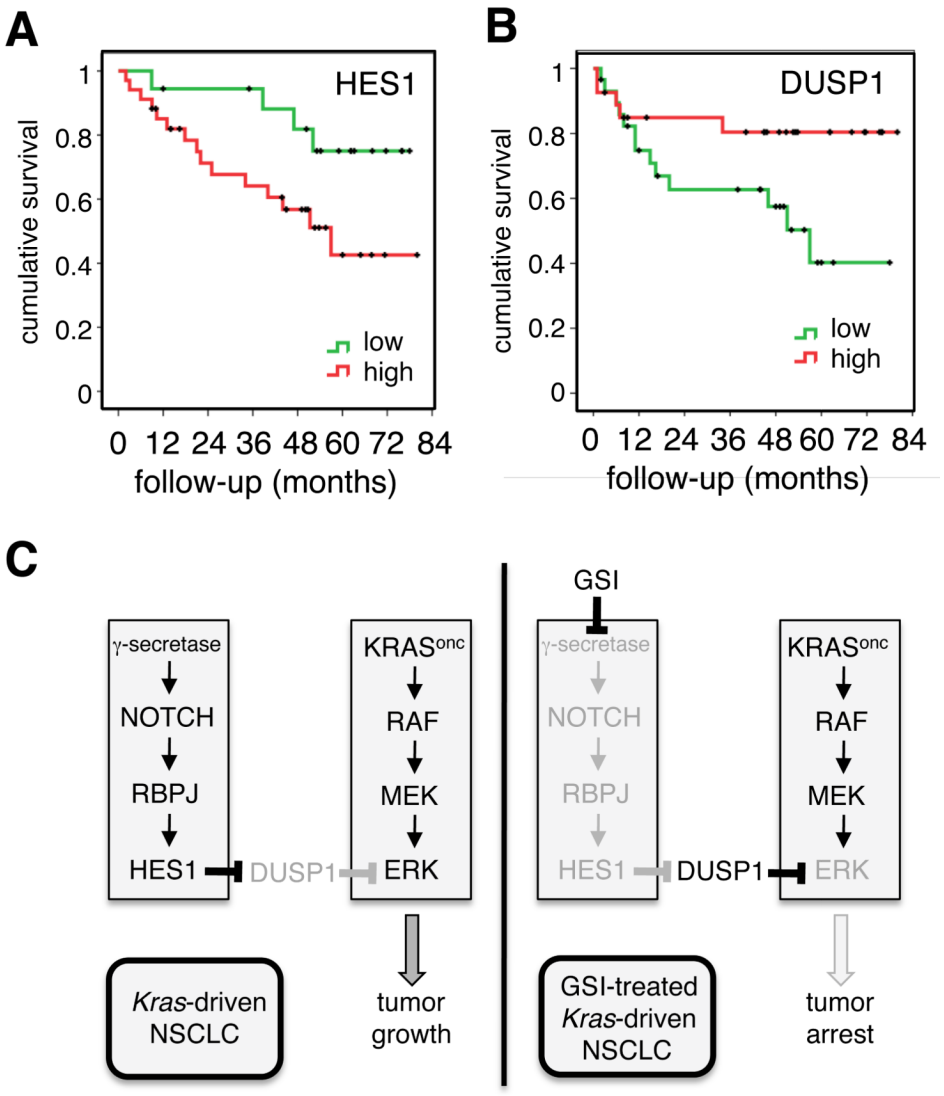

Figure 8. High HES1 and low DUSP1 levels are associated with poor clinical outcome in primary human NSCLCs

(A) Kaplan-Meier curve indicating that tumors displaying high expression of nuclear HES1 show shorter overall survival (p=0.045). High nuclear HES1 expression corresponds to tumors with at least 40% of their neoplastic cells positive for HES1.

(B) Kaplan-Meier curve indicating that tumors displaying low expression of cytoplasmic DUSP1 show poorer overall survival (p=0.048). Low cytoplasmic DUSP1 expression corresponds to tumors with less than 70% of their neoplastic cells positive for DUSP1.

(C) Summary of the data presented in this work. See Discussion for detailed explanation. Logrank test was used to determine statistical significance.

See also Figure S7.